

UC Berkeley

UC Berkeley Previously Published Works

Title

Plasma electron contribution to beam emittance growth from Coulomb collisions in plasma-based accelerators

Permalink

<https://escholarship.org/uc/item/8vv7d3bp>

Journal

Physics of Plasmas, 29(10)

ISSN

1070-664X

Authors

Zhao, Y

Lehe, R

Myers, A

et al.

Publication Date

2022-10-01








DOI

10.1063/5.0102919

Peer reviewed

RESEARCH ARTICLE | OCTOBER 27 2022

Plasma electron contribution to beam emittance growth from Coulomb collisions in plasma-based accelerators

Y. Zhao ; R. Lehe ; A. Myers ; M. Thévenet ; A. Huebl ; C. B. Schroeder ; J.-L. Vay 




Phys. Plasmas 29, 103109 (2022)

<https://doi.org/10.1063/5.0102919>

 CHORUS



CrossMark



International Journal of Fluid Engineering
国际流体工程

No Article Processing Charges (APCs)
Diamond Open Access



Plasma electron contribution to beam emittance growth from Coulomb collisions in plasma-based accelerators

Cite as: Phys. Plasmas **29**, 103109 (2022); doi: 10.1063/5.0102919

Submitted: 13 June 2022 · Accepted: 23 September 2022 ·

Published Online: 27 October 2022



View Online



Export Citation



CrossMark

Y. Zhao,^{1,a)} R. Lehe,¹ A. Myers,¹ M. Thévenet,² A. Huebl,¹ C. B. Schroeder,^{1,3} and J.-L. Vay¹

AFFILIATIONS

¹Lawrence Berkeley National Laboratory, Berkeley, California 94720, USA

²Deutsches Elektronen-Synchrotron, Notkestr. 85, 22607 Hamburg, Germany

³Department of Nuclear Engineering, University of California, Berkeley, California 94720, USA

^{a)} Author to whom correspondence should be addressed: yinjianzhao@lbl.gov

ABSTRACT

Coulomb collisions with background plasma can cause emittance growth in plasma accelerators. This paper extends the theory to consider collisions with not only motionless plasma ions but also plasma electrons with relativistic motion, based on the Frankel cross section. The theory is verified by particle-in-cell simulations with a Monte Carlo collision module. It is shown that the electron contribution has the same amount as that of ions in linear acceleration regime and may not be negligible in nonlinear regime depending on the plasma electron density and its relativistic bulk velocity.

Published under an exclusive license by AIP Publishing. <https://doi.org/10.1063/5.0102919>

I. INTRODUCTION

Preserving beam quality is a key requirement for future plasma-based accelerators. In particular, for prospective plasma-based colliders,¹ preservation of the beam emittance is of great importance, since this quantity eventually determines the beam size and luminosity at the interaction point. This of course holds true both for the electron and positron accelerated beams, in the case of an electron-positron collider. In practice, however, several physical effects can degrade the emittance during acceleration,² including the decoherence of a mismatched beam,^{3,4} misaligned beam,^{3,5} non-linear focusing fields,^{6–8} and the beam-hosing instability.^{9–14} Additionally, Coulomb scattering of the beam particles by the background plasma ions and plasma electrons can also lead to emittance degradation. This is especially true for positron beams, since many proposed plasma-based acceleration schemes require the positron beam to be placed in an area of the wakefield where the plasma electron density is high.^{15–18}

The theoretical study of emittance growth due to Coulomb collisions in plasma-based accelerators was first introduced by Montague and Schnell in 1985.¹⁹ Later, the theory was applied to the blow-out beam-driven regime²⁰ and the quasi-linear laser-driven regime,¹ including in near-hollow plasma channels.²¹ In 2020, Zhao *et al.* extended the theory from a monoenergetic matched beam to a mismatched beam

with energy spread and showed that the emittance growth due to Coulomb collisions can be correctly captured in particle-in-cell simulations, with a proper Monte Carlo binary collision module.²²

The above-mentioned studies only consider collisions with background plasma ions, because collisions with plasma electrons were thought to be negligible. In this paper, we further extend the theory to include collisions with plasma electrons and show that the emittance growth caused by it can be as important as collisions with plasma ions, under some circumstances. We also show that, unlike collisions with motionless ions, collisions with plasma electrons require the electron motion in the wakefield to be taken into account for the theoretical description to be accurate.

The paper is organized as follows. In Sec. II, we derive the contribution of plasma electrons to the emittance growth. In Sec. III, we compare this formula to numerical simulations both in the linear and nonlinear wakefield regimes. Finally, the paper is summarized in Sec. IV.

II. THEORY

We consider an ultra-relativistic beam (consisting either of positrons or electrons) propagating through a background of plasma electrons. In this configuration, the increase in divergence for the beam particles, due to Coulomb scattering, is given by a known formula^{22,23}

(which itself results from the application of the relativistic Frankel cross section²⁴ in the center-of-mass frame of the collision),

$$\frac{d\langle\theta_x^2\rangle}{dt} = \frac{4\pi n_e r_e^2 \gamma_c p'_e}{\gamma_b \gamma_e (\gamma_e + \gamma_b) m_e} \left(\frac{\gamma'_b \gamma'_e m_e^2 c^2}{p_b'^2} + 1 \right)^2 \ln \Lambda_e. \quad (1)$$

In the above formula, the subscript *b* denotes the beam quantities and the subscript *e* denotes the plasma electron quantities, the brackets $\langle \dots \rangle$ indicate an average over scattering events, *p* is the relativistic momentum, *m_e* is the electron rest mass, γ is the Lorentz factor, *n_e* is the number density, *r_e* is the classical electron radius, *c* is the speed of light, and $\ln \Lambda_e$ is the Coulomb logarithm associated with collisions between beam particles and plasma electrons. Primed quantities are taken in the center-of-mass frame of the collision, unprimed quantities are taken in the laboratory frame, and γ_c is the Lorentz factor associated with the center-of-mass frame.

To obtain the corresponding divergence rate in the laboratory frame, we perform a Lorentz transformation under some additional hypotheses. Namely, we neglect transverse motion of the plasma electrons (which is usually valid close to the center of the beam), and assume that the longitudinal motion is mildly relativistic ($\gamma_e \ll \gamma_b$), and that the incident beam particles have low divergence. Under these conditions, we obtain (see the Appendix for a derivation)

$$\frac{d\langle\theta_x^2\rangle}{dt} = \frac{\pi n_e c r_e^2 (1 - \beta_{e,z})}{(\gamma_b + \gamma_e)^2} \left(2 + \frac{\gamma_e (1 + \beta_{e,z})}{\gamma_b} \right)^2 \ln \Lambda_e, \quad (2)$$

where $\beta_{e,z} \equiv v_{e,z}/c$ is the normalized, longitudinal velocity of plasma electrons in the laboratory frame.

Note that, in the above formula, the average corresponds to considering many independent instances of a single electron experiencing a random scattering event. Under the assumption that each electron in the beam experiences independent scattering events, the above average is equivalent to averaging over the particles in the beam. Therefore, in the rest of this paper, the notation $\langle \dots \rangle$ corresponds to an average over beam particles.

To obtain the total rate of emittance growth, we consider the additional contribution from the plasma ions²²

$$\frac{d\langle\theta_x^2\rangle}{dt} = \frac{4\pi n_i c r_e^2}{\gamma_b^2} Z^2 \ln \Lambda_i, \quad (3)$$

where *n_i* is the density of the plasma ions, *Z* is their charge number, and $\ln \Lambda_i$ is the Coulomb logarithm associated with collisions between beam particles and plasma ions. We then follow a similar derivation as in Ref. 22 to obtain the growth of emittance from the increase in divergence. Finally, we further assume that the beam remains adiabatically matched, so that $\langle\theta_x^2\rangle = k_\beta^2 \langle x^2 \rangle$ where $k_\beta = \sqrt{\kappa_f / (m_e \gamma_1)} / c$ is the betatron wavevector, and $\kappa_f = \partial f / \partial x$ denotes the gradient of the transverse focusing force $f = e(E_x + cB_y)$ in the wakefield. Under these assumptions, we obtain the full formula for the growth of emittance due to Coulomb scattering:

$$\frac{d\epsilon_x}{dz} = \frac{2\pi n_0 r_e^2}{\gamma_b k_\beta} \left[Z \ln \Lambda_i + \frac{n_e (1 - \beta_{e,z})}{n_0 (1 + \gamma_e / \gamma_b)^2} \left(1 + \frac{\gamma_e (1 + \beta_{e,z})}{2\gamma_b} \right)^2 \ln \Lambda_e \right], \quad (4)$$

where $n_0 = Zn_i$. Note that the first term is the contribution from collisions with plasma ions, and the second term is the contribution from collisions with plasma electrons.

A few remarks can be made on Eq. (4). First, the $1/k_\beta$ dependency is a reminder that strong focusing (i.e., a large k_β) is required to reduce the emittance growth due to collisions.¹ Second, Eq. (4) indicates that the contribution to the emittance growth from the plasma electrons and plasma ions are of the same order of magnitude. In particular, in the limit of an ultra-relativistic beam, i.e., $\gamma_e \ll \gamma_b$, Eq. (4) reduces to

$$\frac{d\epsilon_x}{dz} = \frac{2\pi n_0 r_e^2}{\gamma_b k_\beta} \left[Z \ln \Lambda_i + \frac{n_e}{n_0} (1 - \beta_{e,z}) \ln \Lambda_e \right]. \quad (5)$$

In the linear regime, $n_e/n_0 = 1 + \delta n/n_0$, and $\beta_{e,z} = \delta n/n_0$ with $|\delta n/n_0| \ll 1$. Hence, $(n_e/n_0)(1 - \beta_{e,z}) = (1 + \delta n/n_0)(1 - \delta n/n_0) \approx 1$, and thus, in the case $Z = 1$ and $\ln \Lambda_i \approx \ln \Lambda_e$, the contributions from the ions and electrons are approximately equal. Fundamentally, this is because the Frankel cross section²⁴ assumes instantaneous interaction between the colliding particles, i.e., the particles do not have time to move while interacting, and therefore, the mass of the target species (plasma electron or plasma ions) is irrelevant in the scattering cross section.

Finally, as mentioned in previous work,²⁴ we note that it is difficult to precisely estimate the Coulomb logarithms, and that different prescriptions exist in the literature. In the case of collisions with plasma ions, we use $\ln \Lambda_i = \ln(\lambda_D/R)$, where λ_D is the Debye length and $R = 1.4 A^{1/3}$ fm is the effective Coulombic radius of the nucleus.²² For the parameters considered in this paper (hydrogen plasma with a density $n_0 = 10^{17}$ cm⁻³ and a temperature of 10 eV), this gives $\ln \Lambda_i = 17.8$. In the case of collisions with plasma electrons, we use the prescription of Frankel²⁴ with $b_{\max} = \lambda_D$ as the maximum impact parameter. In the limit of $\gamma_b \gg \gamma_e$, this prescription simplifies to $\ln \Lambda_e = \ln(\lambda_D/r_e \times \sqrt{\gamma_b \gamma_e (1 - \beta_{e,z})/2})$. Although this quantity depends on γ_b and γ_e , this dependency is weak because of the logarithm and square root. For instance, for the same plasma parameters as above and with $\gamma_e \approx 1$, we have $\ln \Lambda_e = 19.4$ for $\gamma_b = 200$ and $\ln \Lambda_e = 21.2$ for $\gamma_e = 8000$. For simplicity, in this paper, we choose a fixed value $\ln \Lambda_e = 20$, both in the theory and simulations.

III. SIMULATION

A. Setup and parameters

In order to verify the predictions of Eq. (5) in a realistic laser-plasma acceleration scenario, we perform particle-in-cell (PIC) simulations of a beam-driven plasma accelerator, using the open-source code WarpX.^{25,26} We consider both a linear wakefield regime (Sec. III B) and a nonlinear wakefield regime (Sec. III C), by varying the charge of the beam driver. Importantly, in either case, we introduce both a witness electron beam and a witness positron beam in the wakefield (at different respective phases), in order to highlight potential differences in the typical growth of emittance experienced by these two types of beam.

In the PIC simulations, the Coulomb collisions between the witness beam particles and the plasma electrons and ions are captured by a Monte Carlo module,²³ which is based on the Frankel cross section.²⁴

All simulations are carried out in a Lorentz-boosted frame²⁷ (with a Lorentz factor $\gamma = 10$) and use the following setup and parameters. A driver electron beam is initialized with a Gaussian distribution

with RMS size $\sigma_x = \sigma_y \approx 6.32 \mu\text{m}$, $\sigma_z \approx 12.65 \mu\text{m}$. We represent the driver with eight macro-particles per cell and set it to propagate rigidly at the speed of light through the plasma. The plasma has a 1 mm density upramp, followed by a 0.5 m plateau at $n_0 = 10^{17} \text{cm}^{-3}$. The plasma electrons and ions are represented with 50 macro-particles per cell, respectively. The ions have a charge number $Z = 1$ and are set to be rigid in the simulation. A 3D cubic simulation domain is used with $128 \times 128 \times 256$ cells in $x, y,$ and z directions and reflective boundary conditions in the transverse dimensions. The physical domain corresponds to a $200 \times 200 \times 256 \mu\text{m}$ box in the lab frame. Both electron and positron witness beams are initialized with Gaussian distributions, with an ultra-low emittance $\varepsilon_x = \varepsilon_y = 20 \text{nm}$, an initial energy corresponding to $\gamma_b = 200$ and a $0.2 \mu\text{m}$ beam length. Their beam size is matched to the focusing plasma wakefield experienced at the beginning of the density plateau. Both electron and positron witness beams are represented by 10^6 macro-particles and have artificially small total charge i.e., 1 fC so that beamloading is negligible. (Note that, in the limit of negligible beamloading, the growth of emittance is in principle independent of the actual charge of the beam.) The simulations use the Cole-Karkkainen Maxwell solver with Cowan coefficients²⁸ and the Boris particle pusher.²⁹ In order to reduce computational cost, the collision module is run only with $20\times$ larger time step than the Maxwell solver (i.e., it is only applied at every 20 iterations of the PIC loop).

In order to isolate the growth of emittance due to Coulomb scattering from that due to the other sources (e.g., slight beam mismatch, coupled with a small energy spread), each simulation was run twice: once with the collision module turned on and once with this module turned off. The emittance growth that we plot (e.g., in Figs. 2 and 4) is the difference between the emittances in this pair of simulations. In addition, because the Monte Carlo collision module and the Gaussian beam initialization are stochastic in nature, the pair of simulations is run several times, while changing the random seed.

B. Linear regime

In order to produce a linear wakefield, we set the charge of the driver to 10 pC. The electron and positron witness beams are separated by half a plasma wavelength, so that they experience symmetric accelerating and focusing fields, as represented in Fig. 1.

To compare the theoretical growth of emittance with the simulations, Eq. (5) can be integrated numerically. Note that, in this case, the values of $\gamma_b, k_\beta,$ and n_e in Eq. (5) are extracted from the simulation. (These values are also shown on the right panel of Fig. 2 for γ_b and in the bottom panel of Fig. 1 for the other quantities.) The resulting emittance growth for the electron and positron witness beams are shown in Fig. 2 (left and middle panels, respectively).

As can be seen from Fig. 2, there is good agreement between Eq. (5) (black dashed line) and the emittance growth extracted from the simulations (solid lines). In this case, the contribution of the plasma electrons account for half of the emittance growth (as shown by the green dashed curve).

In addition, it is worth noting here that the growth of emittance is identical for the electron beam and positron beam, in Fig. 2. This is because (i) the electron and positron beams experience symmetrical accelerating and focusing forces, and (ii) they both propagate through a similar density of plasma electrons. (Given the low amplitude of the wakefield, the density of plasma electrons seen by each beam is very close to n_0 .) This is no longer the case in the nonlinear wakefield regime.

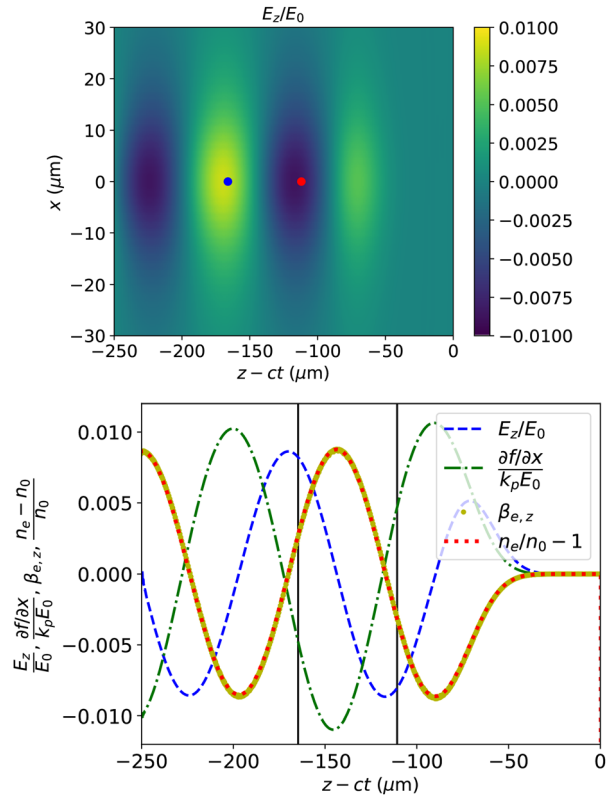


FIG. 1. Snapshots of the wakefield in the linear regime. Top: colormap of the normalized accelerating wakefield E_z/E_0 , where $E_0 = m_e c \omega_p / e$ and ω_p is the plasma frequency. The positions of the positron and electron witness beams are represented by a blue and red dot, respectively. Bottom: on-axis plot of the normalized density n_e , electron velocity $\beta_{e,z}$, accelerating field E_z , and focusing gradient $\partial f / \partial x$. The positions of the electron and positron witness beams are indicated by the two vertical black lines.

C. Nonlinear regime

To simulate a nonlinear regime, the total charge of the driver beam is set to 160 pC. The wakefield and the positions of the electron and positron beams are represented in Fig. 3. In particular, the positron beam is placed within the narrow region in which the wakefield is both accelerating and focusing. Note that, as shown in the bottom panel of Fig. 3, this also corresponds to a region where the density and velocity of the plasma electrons is high. By contrast, for the electron beam, the accelerating and focusing region corresponds to a region where the density of plasma electrons is close to zero.

We note that, in the nonlinear case, it is crucial to use a sufficient number of macroparticles for the plasma electrons. This is because the Monte Carlo collision algorithm internally evaluates the local plasma electron density by binning macro-particles into cells. Thus, there needs to be enough macroparticles to ensure that the (discrete) count of macroparticles in a cell is representative of the actual (continuous) plasma density in the wakefield. Here, as for the linear case, we use 50 macroparticles per cell for the plasma. The electron density represented in Fig. 3 [and used when integrating Eq. (5)] is also obtained by

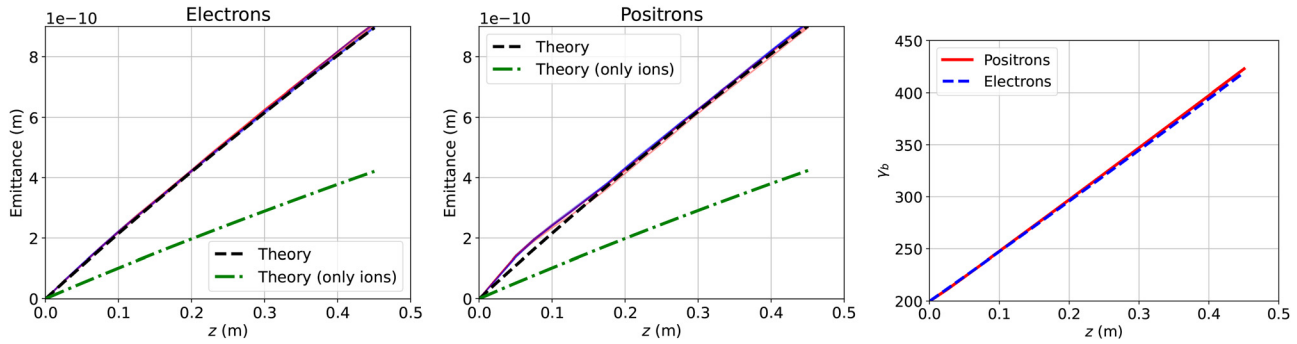


FIG. 2. Left and middle panels: emittance growth of the electron and positron witness beam due to Coulomb scattering. The black dashed lines show the result of numerically integrating Eq. (5), while the solid lines show the growth of emittance extracted from the simulation directly (with ε_x in red and ε_y in blue). Note that there are 5 blue lines and 5 red lines, which correspond to five separate simulations with different random seeds, giving a measure of the uncertainty associated with the stochastic nature of the Monte Carlo collision module. For comparison, the green dashed lines show the result of neglecting the plasma electrons in Eq. (5). Right panel: evolution of the Lorentz factors of the electron and positron witness beams throughout the simulation.

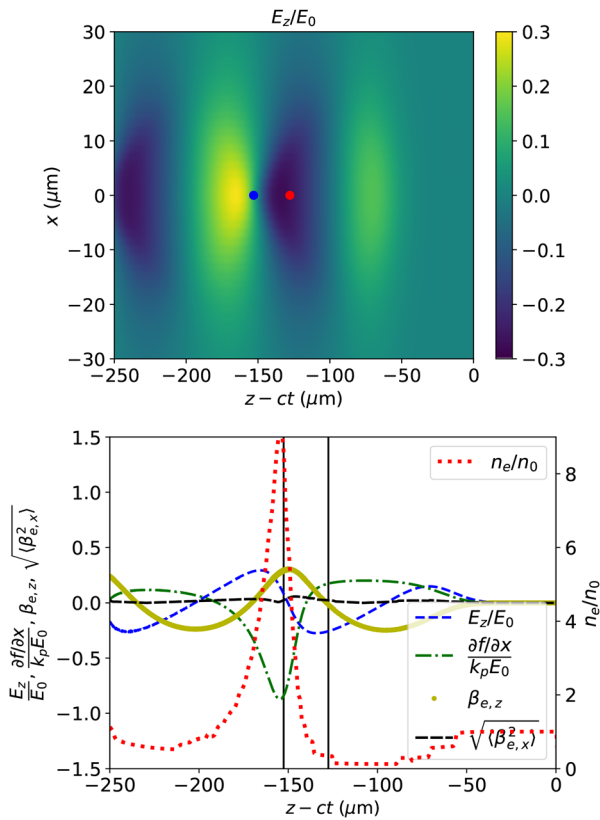


FIG. 3. Snapshots of the wakefield in the nonlinear regime. Top: colormap of the normalized accelerating wakefield E_z/E_0 , where $E_0 = m_e c \omega_p / e$ and ω_p is the plasma frequency. The positions of the positron and electron witness beams are represented by a blue and red dot, respectively. Bottom: on-axis plot of the normalized density n_e , longitudinal electron velocity $\beta_{e,z}$, accelerating field E_z , focusing gradient $\partial f / \partial x$, and the RMS transverse velocity $\sqrt{\langle \beta_{e,x}^2 \rangle}$. The positions of the electron and positron witness beams are indicated by the two vertical black lines.

binning macro-particles into cells and confirms that, in this case, there are enough macroparticles for this curve to be smooth.

In addition, one of the assumptions made in the theory is that the transverse motion of the plasma electrons is neglected. This assumption is valid in the regime investigated, as indicated by the curve corresponding to $\sqrt{\langle \beta_{e,x}^2 \rangle}$ in Fig. 3: overall, $\sqrt{\langle \beta_{e,x}^2 \rangle}$ remains very low on axis, in the wakefield.

The theoretical prediction of Eq. (5) (black dashed lines) is compared with the emittance extracted from the simulation (solid lines) in Fig. 4 and shows good agreement. We note that the emittance growth is higher for the positron beam than for the electron beam. This is due to the fact that the positrons experience a lower accelerating field (which results in a lower γ_b) and to a higher plasma electron density n_e (which increases the contribution from the plasma electrons to Coulomb scattering).

The contribution of the plasma ions to the emittance [i.e., the first term in Eq. (5)] is represented by the red dotted curve in the left and middle panels of Fig. 4. As can be seen, the contribution of the plasma ions dominates in the case of the electron beam (left panel), and this is because the electron beam propagates in a region of wakefield that is almost void of plasma electrons (see Fig. 3). On the other hand, the contribution of the plasma ions is small compared to that of the plasma electrons for the positrons beam (middle panel), since the positron beam is located in an area of high electron density.

Finally, the middle panel of Fig. 4 shows that it is important to take into account the relativistic motion of the plasma electrons when predicting the growth of emittance for the positron beam. The green dashed curve indeed shows that the simulation data are incompatible with Eq. (5) when $\beta_{e,z}$ is set to zero, which neglects this relativistic motion. In this case, the fully relativistic equation results in a lower growth of emittance mainly because of the factor $(1 - \beta_{e,z})$, which multiplies the plasma electron density n_e . This effect is much less pronounced for the electron beam, since it propagates in a region of the wakefield where $\beta_{e,z}$ is close to 0 (see Fig. 3).

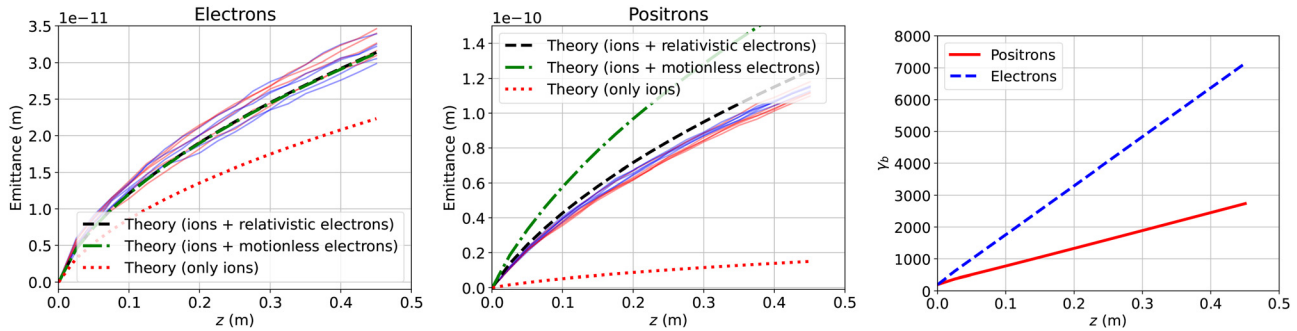


FIG. 4. Left and middle panels: emittance growth of the electron and positron witness beam due to Coulomb scattering. The black dashed lines show the result of numerically integrating Eq. (5), while the solid lines show the growth of emittance extracted from the simulation directly (with ϵ_x in red and ϵ_y in blue). Note that there are 5 blue lines and 5 red lines, which correspond to five separate simulations with different random seeds, giving a measure of the uncertainty associated with the stochastic nature of the Monte Carlo collision module. The green dashed lines show the result of integrating Eq. (5) with $\beta_{e,z} = 0$. The red dashed lines show the result of neglecting the plasma electrons in Eq. (5). Right panel: evolution of the Lorentz factors of the electron and positron witness beams throughout the simulation.

IV. CONCLUSION

This paper generalizes the theory of beam emittance growth due to Coulomb collisions with background plasma electrons in plasma-based accelerators. The generalized theoretical formula is verified with particle-in-cell simulations incorporating a Monte Carlo collision module. The theory and the simulation results indicate that the emittance growth due to the plasma electrons can be of the same order of magnitude as that due to the plasma ions. In addition, these results show that the relativistic motion of the electrons need to be taken into account in order to accurately calculate the growth of emittance. This is particularly true for positron beams, since they often need to be placed in a region of the wakefield where both the density and velocity of the plasma electrons are high.

ACKNOWLEDGMENTS

The authors would like to thank all WarpX contributors. This work was supported by the Exascale Computing Project (No. 17-SC-20-SC), a collaborative effort of the U.S. Department of Energy Office of Science and the National Nuclear Security Administration. This work was also supported by the Director, Office of Science, Office of High Energy Physics, U.S. Dept. of Energy under Contract No. DEAC02-05CH11231. This research used resources of the Oak Ridge Leadership Computing Facility at the Oak Ridge National Laboratory, which is supported by the Office of Science of the U.S. Department of Energy under Contract No. DE-AC05-00OR22725.

AUTHOR DECLARATIONS

Conflict of Interest

The authors have no conflicts to disclose.

Author Contributions

Yinjian Zhao: Conceptualization (equal); Data curation (equal); Methodology (equal); Software (equal); Validation (equal); Visualization (equal); Writing – original draft (equal); Writing – review & editing (equal). **Rémi Lehe:** Conceptualization (equal); Supervision (equal); Writing – review & editing (equal). **Andrew Myers:** Software (equal); Writing – review & editing (equal). **Maxence Thevenet:** Software (equal); Writing – review & editing (equal).

Axel Huebl: Software (equal); Writing – review & editing (equal). **Carl Schroeder:** Conceptualization (equal); Methodology (equal); Validation (equal); Writing – review & editing (equal). **Jean-Luc Vay:** Supervision (equal); Writing – review & editing (equal).

DATA AVAILABILITY

The data that support the findings of this study is openly available in Zenodo at <https://doi.org/10.5281/zenodo.7035859>, Ref. 30.

APPENDIX: DERIVATION OF EMITTANCE GROWTH DUE TO COLLISIONS WITH PLASMA ELECTRONS

In this section, we show how to convert Eq. (1), into Eq. (2), so that it only involves quantities that are taken in the laboratory frame. We consider a collision between a beam particle (either a positron or an electron) with momentum $\mathbf{p}_b = \gamma_b m_e \mathbf{v}_b$ (with $\gamma_b \gg 1$) and an electron of the background plasma with momentum $\mathbf{p}_e = \gamma_e m_e \mathbf{v}_e$. We assume that the plasma electron is mildly relativistic (in particular $\gamma_e \ll \gamma_b$) and moves purely along the direction of beam propagation z . We also assume that the beam particle is ultra-relativistic ($\gamma_b \gg 1$) and has a small angle in x ($p_{b,x} \approx \gamma_b m_e c \theta_x$, $p_{b,z} \approx \gamma_b m_e c$).

The Lorentz transformation between the center-of-mass frame²³ and laboratory is determined by the center-of-mass velocity

$$\mathbf{v}_c = \frac{\mathbf{p}_b + \mathbf{p}_e}{m_e(\gamma_b + \gamma_e)}. \tag{A1}$$

Given that \mathbf{p}_b and \mathbf{p}_e have either a zero or negligible component along x , we make the approximation that \mathbf{v}_c is purely along z . Because $\gamma_e \ll \gamma_b$, we also consider that v_{cz} is close to c (i.e., the corresponding Lorentz factor satisfies $\gamma_c \gg 1$), given that the incident beam particle is ultra-relativistic.

In this case, the Lorentz transformation of the four-momentum of the beam particle gives

$$\gamma'_b = \gamma_c \left[\gamma_b - \frac{v_{cz} p_{b,z}}{m_e c^2} \right] \approx \gamma_c \left[\gamma_b - \left(1 - \frac{1}{2\gamma_c^2} \right) \gamma_b \right] \approx \frac{\gamma_b}{2\gamma_c}, \tag{A2}$$

$$p'_{b,x} = p_{b,x} = \gamma_b m_e c \theta_x, \tag{A3}$$

$$p'_{b,z} = \gamma_c [\gamma_b p_{b,z} - v_{cz} \gamma_b m_e] \approx \frac{\gamma_b m_e c}{2\gamma_c}. \tag{A4}$$

From the above equations, we can extract the relationship between the incidence angle in the center-of-mass frame and laboratory frame, which is to be used in the right-hand side of Eq. (1)

$$\theta'_x \approx \frac{p'_{b,x}}{p'_{b,z}} \approx 2\gamma_c \theta_x. \tag{A5}$$

Similarly, the Lorentz transformation of the four-momentum of the plasma particle gives

$$\gamma'_e \approx \gamma_c \gamma_e \left[(1 - \beta_{e,z}) + \frac{1}{2\gamma_c^2} \right], \tag{A6}$$

$$p'_{e,z} \approx \gamma_c \gamma_e m_e c \left[-(1 - \beta_{e,z}) + \frac{1}{2\gamma_c^2} \right]. \tag{A7}$$

We can now express γ_c as a function of the other quantities, by using the fact that, in the center-of-mass frame, $p'_{b,z} + p'_{e,z} = 0$, along with Eqs. (A4) and (A7), we have

$$\gamma_c^2 \approx \frac{(\gamma_b + \gamma_e)}{2\gamma_e(1 - \beta_{e,z})}. \tag{A8}$$

By using Eqs. (A2), (A4), (A5), (A6), and (A8) in Eq. (1), Eq. (2) can be obtained.

REFERENCES

- ¹C. B. Schroeder, E. Esarey, C. G. R. Geddes, C. Benedetti, and W. P. Leemans, "Physics considerations for laser-plasma linear colliders," *Phys. Rev. Spec. Top.- Accel. Beams* **13**, 101301 (2010).
- ²C. Lindström and M. Thévenet, "Emittance preservation in advanced accelerators," *J. Instrum.* **17**, P05016 (2022).
- ³P. Michel, C. B. Schroeder, B. A. Shadwick, E. Esarey, and W. P. Leemans, "Radiative damping and electron beam dynamics in plasma-based accelerators," *Phys. Rev. E* **74**, 026501 (2006).
- ⁴T. Mehrling, J. Grebenyuk, F. S. Tsung, K. Floettmann, and J. Osterhoff, "Transverse emittance growth in staged laser-wakefield acceleration," *Phys. Rev. Spec. Top.- Accel. Beams* **15**, 111303 (2012).
- ⁵M. Thévenet, R. Lehe, C. B. Schroeder, C. Benedetti, J.-L. Vay, E. Esarey, and W. P. Leemans, "Emittance growth due to misalignment in multistage laser-plasma accelerators," *Phys. Rev. Accel. Beams* **22**, 051302 (2019).
- ⁶J. B. Rosenzweig, A. M. Cook, A. Scott, M. C. Thompson, and R. B. Yoder, "Effects of ion motion in intense beam-driven plasma wakefield accelerators," *Phys. Rev. Lett.* **95**, 195002 (2005).
- ⁷W. An, W. Lu, C. Huang, X. Xu, M. J. Hogan, C. Joshi, and W. B. Mori, "Ion motion induced emittance growth of matched electron beams in plasma wakefields," *Phys. Rev. Lett.* **118**, 244801 (2017).
- ⁸C. Benedetti, C. B. Schroeder, E. Esarey, and W. P. Leemans, "Emittance preservation in plasma-based accelerators with ion motion," *Phys. Rev. Accel. Beams* **20**, 111301 (2017).
- ⁹Y. Y. Lau, "Classification of beam breakup instabilities in linear accelerators," *Phys. Rev. Lett.* **63**, 1141-1144 (1989).
- ¹⁰A. W. Chao, B. Richter, and C.-Y. Yao, "Beam emittance growth caused by transverse deflecting fields in a linear accelerator," *Nucl. Instrum. Methods* **178**, 1-8 (1980).

- ¹¹A. A. Geraci and D. H. Whittum, "Transverse dynamics of a relativistic electron beam in an underdense plasma channel," *Phys. Plasmas* **7**, 3431-3440 (2000).
- ¹²E. S. Dodd, R. G. Hemker, C.-K. Huang, S. Wang, C. Ren, W. B. Mori, S. Lee, and T. Katsouleas, "Hosing and sloshing of short-pulse GeV-class wakefield drivers," *Phys. Rev. Lett.* **88**, 125001 (2002).
- ¹³C. B. Schroeder, D. H. Whittum, and J. S. Wurtele, "Multimode analysis of the hollow plasma channel wakefield accelerator," *Phys. Rev. Lett.* **82**, 1177-1180 (1999).
- ¹⁴C. Huang, W. Lu, M. Zhou, C. E. Clayton, C. Joshi, W. B. Mori, P. Muggli, S. Deng, E. Oz, T. Katsouleas, M. J. Hogan, I. Blumenfeld, F. J. Decker, R. Ischebeck, R. H. Iverson, N. A. Kirby, and D. Walz, "Hosing instability in the blow-out regime for plasma-wakefield acceleration," *Phys. Rev. Lett.* **99**, 255001 (2007).
- ¹⁵S. Corde, E. Adli, J. M. Allen, W. An, C. I. Clarke, J. P. Delahaye, J. Frederico, S. Gessner, S. Z. Green, M. J. Hogan, C. Joshi, N. Lipkowitz, M. Litos, W. Lu, K. A. Marsh, W. B. Mori, M. Schmeltz, N. Vafaei-Najafabadi, D. Walz, V. Yakimenko, G. Yocky, and C. E. Clayton, "Multi-gigaelectronvolt acceleration of positrons in a self-loaded plasma wakefield," *Nature* **524**, 442-445 (2015).
- ¹⁶T. Wang, V. Khudik, and G. Shvets, "Positron acceleration in an elongated bubble regime," [arXiv:2110.10290](https://arxiv.org/abs/2110.10290) (2021).
- ¹⁷S. Diederichs, T. J. Mehrling, C. Benedetti, C. B. Schroeder, A. Knetsch, E. Esarey, and J. Osterhoff, "Positron transport and acceleration in beam-driven plasma wakefield accelerators using plasma columns," *Phys. Rev. Accel. Beams* **22**, 081301 (2019).
- ¹⁸J. Vieira and J. T. Mendonça, "Nonlinear laser driven donut wakefields for positron and electron acceleration," *Phys. Rev. Lett.* **112**, 215001 (2014).
- ¹⁹B. W. Montague and W. Schnell, "Multiple scattering and synchrotron radiation in the plasma beat-wave accelerator," *AIP Conf. Proc.* **130**, 146-155 (1985).
- ²⁰N. Kirby, M. Berry, I. Blumenfeld, M. J. Hogan, R. Ischebeck, and R. Siemann, "Emittance growth from multiple Coulomb scattering in a plasma wakefield accelerator," in *IEEE Particle Accelerator Conference (PAC)* (IEEE, 2007) pp. 3097-3099.
- ²¹C. B. Schroeder, E. Esarey, C. Benedetti, and W. P. Leemans, "Control of focusing forces and emittances in plasma-based accelerators using near-hollow plasma channels," *Phys. Plasmas* **20**, 080701 (2013).
- ²²Y. Zhao, R. Lehe, A. Myers, M. Thévenet, A. Huebl, C. B. Schroeder, and J.-L. Vay, "Modeling of emittance growth due to Coulomb collisions in plasma-based accelerators," *Phys. Plasmas* **27**, 113105 (2020).
- ²³F. Pérez, L. Gremillet, A. Decoster, M. Drouin, and E. Lefebvre, "Improved modeling of relativistic collisions and collisional ionization in particle-in-cell codes," *Phys. Plasmas* **19**, 083104 (2012).
- ²⁴N. E. Frankel, K. C. Hines, and R. L. Dewar, "Energy loss due to binary collisions in a relativistic plasma," *Phys. Rev. A* **20**, 2120-2129 (1979).
- ²⁵J.-L. Vay, A. Almgren, J. Bell, L. Ge, D. P. Grote, M. Hogan, O. Kononenko, R. Lehe, A. Myers, C. Ng, J. Park, R. Ryne, O. Shapoval, M. Thévenet, and W. Zhang, "Warp-X: A new exascale computing platform for beam-plasma simulations," [arXiv:1801.02568](https://arxiv.org/abs/1801.02568) (2018).
- ²⁶A. Myers, A. Almgren, L. Amorim, J. Bell, L. Fedeli, L. Ge, K. Gott, D. Grote, M. Hogan, A. Huebl, R. Jambunathan, R. Lehe, C. Ng, M. Rowan, O. Shapoval, M. Thévenet, J.-L. Vay, H. Vincenti, E. Yang, N. Zaim, W. Zhang, Y. Zhao, and E. Zoni, "Porting WarpX to GPU-accelerated platforms," *Comput.* **108**, 102833 (2021).
- ²⁷J.-L. Vay, "Noninvariance of space- and time-scale ranges under a Lorentz transformation and the implications for the study of relativistic interactions," *Phys. Rev. Lett.* **98**, 130405 (2007).
- ²⁸B. M. Cowan, D. L. Bruhwiler, J. R. Cary, E. Cormier-Michel, and C. G. R. Geddes, "Generalized algorithm for control of numerical dispersion in explicit time-domain electromagnetic simulations," *Phys. Rev. Spec. Top. Accel. Beams* **16**, 041303 (2013).
- ²⁹C. K. Birdsall and A. B. Langdon, *Plasma Physics via Computer Simulation* (IOP, 1991).
- ³⁰Y. Zhao and R. Lehe (2020). "Plasma electron contribution to beam emittance growth from coulomb collisions in plasma-based accelerators," [Zenodo, Dataset](https://zenodo.org/record/4000000).